

# Determination of the Ar/Ca solar wind elemental abundance ratio using SOHO/CELIAS/MTOF

J. M. Weygand\*, F. M. Ipavich<sup>†</sup>, P. Wurz\*\*, J.A. Paquette<sup>†</sup> and P. Bochsler\*\*

\*IGPP/UCLA 3845 Slichter Hall, Los Angeles, CA, 90095-1567, USA

<sup>†</sup>University of Maryland, College Park, MD 20742, USA

\*\*Physikalisches Institute, University of Bern, Sidlerstrasse 5, CH-3012, Bern, Switzerland

## Abstract.

This study examines the first direct measurements of the solar wind (SW) Ar/Ca elemental abundance ratio with the Mass Time-Of-Flight (MTOF) sensor of the Charge, Element, and Isotope Analysis System (CELIAS) instrument on the Solar and Heliospheric Observatory (SOHO) spacecraft. Two mass spectra are compiled for interstream (IS) associated SW and coronal hole (CH) associated SW. A detailed analysis of over 3.6 days of non-consecutive IS associated SW speed ( $395 \pm 25$  km/s) places the Ar/Ca elemental ratio at  $0.38 \pm 0.05$ . A similar analysis for CH associated SW speed ( $525 \pm 25$  km/s), with about 5.6 non-consecutive days of CH associated SW speed data, derived an Ar/Ca ratio of  $0.59 \pm 0.07$ . The results of this study are consistent with most previously published Ar/Ca values from gradual solar energetic particle events and spectroscopy studies.

## INTRODUCTION

It has been observed in the solar wind (SW) that elements with a low first ionization potential (FIP  $< 10$  eV) are enriched relative to elements with a high FIP (i.e., FIP  $> 10$  eV) as compared to elements in the photosphere using oxygen as a reference ( $[X/O]_{SW}/[X/O]_{photosphere}$ ). The enrichment in the interstream (IS) associated SW is about two to five for the low FIP elements and around one for the high FIP elements. It is generally believed that the relative enrichments are due to a fractionation process in the upper chromosphere and lower transition zone and are the result of neutral-ion separation with ionization most likely caused by EUV radiation from the solar corona.

The high FIP element argon (FIP = 15.76 eV) is highly volatile and of low abundance in the SW. Because of argon's volatility, inferences about the solar and solar system argon abundance from planetary samples are problematic. Calcium is a low FIP (FIP = 6.11 eV) species and a refractory element, which is moderately abundant in the SW compared to argon. The present measurements are selected with the goal of obtaining accurate information on the present day solar atmosphere elemental composition. Furthermore, the Sun represents 99.9% of the solar system's matter, and since the Sun's central temperature has never been high enough to alter the elemental composition of the heavy elements by nuclear reactions, an accurate elemental composi-

tion measurement should reflect the pre-solar nebula elemental composition. Until recently, direct measurements of the IS and coronal hole (CH) associated SW argon and calcium composition have not been possible. Previously reported Ar/Ca elemental abundance ratio values were determined through 1) gradual SEP event measurements, 2) the corona and photosphere emission spectra in a variety of wavelength regimes, 3) the Apollo missions foil experiments, and 4) through meteoritic samples [1, 2, 3, 4]. While the above methods are accurate for the measurements made, those methods do not directly sample the IS and CH associated SW nor do these measurements tie the argon abundance to a refractory element. Direct measurements may provide limits to the variability of elemental abundance ratios within different SW regimes, and hence, obtain a clue on the importance of fractionation effects occurring in the SW. As of the late 1990's, several different composition instruments, such as WIND/SMS, SOHO/CELIAS, ACE/SWIMS, and ACE/SWICS [5, 6, 7], made it possible to determine the solar elemental composition quite reliably from direct SW observations [8, 9, 10]. Recent argon isotopic ratio measurements have demonstrated that both  $^{36}\text{Ar}$  and  $^{38}\text{Ar}$  can be successfully detected in the SW [11]. Calcium solar elemental composition measurements, on the other hand, have been extensively reported, but only recently have measurements come directly from the SW [8, 9].

Recent statistical measurements of the Fe/O elemental abundance ratio in the SW over all SW speeds have shown three compositional regions [10, 9]. The first of these regions is a slow speed SW for speeds less than 400 km/s, where the elemental abundance ratio appears to plateau. The second region is the highest speed bin for speeds above 500 km/s, where the elemental abundance ratio again looks constant. These two regimes are IS associated SW and CH associated SW, respectively. For the speeds in between (i.e., 400 km/s to 500 km/s), the elemental abundance ratio seems to monotonically decrease from slow speeds to high speeds. Furthermore, it was demonstrated that there is approximately a factor of two difference in the Fe/O ratio between the IS associated SW (i.e., < 400 km/s) and the CH associated SW (i.e., > 500 km/s) [10, 9].

This study determines the Ar/Ca ratio with the Mass Time-Of-Flight (MTOF) sensor of the Charge, Element, and Isotope Analysis System (CELIAS) instrument on the Solar and Heliospheric Observatory (SOHO) spacecraft for both the IS associated SW and the CH associated SW. For details on the MTOF sensor and CELIAS instrument see the work of Hovestadt et al. [6].

## PROCEDURE

The most important criterion for the data selection is a high signal-to-noise ratio (SNR) for the argon. Unlike previous CELIAS/MTOF investigations, where the SNR is anywhere from about four to a few orders of magnitude, the SNR for  $^{36}\text{Ar}$  is around 1.1 and about 1.8 for  $^{40}\text{Ca}$ . To further complicate matters, additional constraints had to be imposed on the data set. The first of these constraints concerns data binning into either IS or CH associated SW. The IS associated SW sample contains SW speeds between 370 km/s and 420 km/s, and the CH associated SW bin lies between 500 km/s and 550 km/s. The two SW ranges precise location is derived from instrumentation requirements and from previous composition studies [10, 9, 12]. The two SW bins are selected such that they mostly lie in the two compositionally separate SW regimes previously observed [10, 9], which, in this study, we refer to as IS associated SW (SW < 400 km/s) and CH associated SW (SW > 500 km/s). While it is true that the IS associated SW speed bin is not entirely below 400 km/s, some leeway is allowed to improve the argon peak's SNR. Finally, the SW bins are also selected to be similar to those of the Weygand et al. [11] study so we may unambiguously determine the total argon counts in the  $^{38}\text{Ar}$  peaks. In addition to restricting the speed, the SW's duration is required to be a minimum of 12 hours for the IS associated bin and a minimum of 6 hours for the CH associ-

ated SW bin. This minimum duration criterion limits the data set to large-scale and uniform flows as well as excludes variable speed flows, which would possibly mix results from the two SW regimes. Also not included in the mass spectra are data associated with CME's, shocks, and corotating interaction regions, since the passage of a CME can have markedly different elemental composition [13, 14, 15].

For the second constraint, the only instrument settings considered are those which allowed argon and calcium to pass through the MTOF sensor in a very similar manner. The two bins need to be in a region of high transmission for the time of flight (TOF) portion of the MTOF sensor as well as in the region of maximum effective carbon foil area as determined by the wide-angle, variable energy/charge (WAVE) entrance system. While these constraints restrict the total amount of data, they guarantee that Ar and Ca are treated nearly identically by the instrument.

SW argon and calcium enter the MTOF sensor through the WAVE system. The WAVE section consists of three energy over charge selection chambers. The entrance system allows a large energy range of ions to enter the sensor through a wide angular acceptance cone. Particles, which pass through this region, cross through a carbon foil, which reduces their charge from some initial SW charge distribution (i.e., +8, +9, and +10 for argon and +9, +10, +11, and +12 for calcium) to neutral, +1, or +2, where the most probable ion charge is +1 [16]. Argon and calcium essentially pass through the WAVE system in the same way with one assumption. If the argon and calcium ion's speed is about the same, then their nearly identical passage is determined by their M/Q SW value, which is four for both ions when we use their most probable charge state in a SW (i.e., +9 for argon and +10 for calcium) of a freeze-in temperature of 1.4 MK. The results vary at maximum by about 5% when other less probable charge states are examined. This 5% will be used as our uncertainty in the WAVE portion of the MTOF sensor. After the carbon foil, the ions follow a hyperbolic path through the TOF portion of MTOF to the ion MCP detector where they are recorded as counts.

Figure 1 is a plot of the argon and calcium total transmission through the TOF section of MTOF, where the transmission is calculated with a forward model [12]. The transmission curve has been compared with ground calibration data and there is a good agreement between the two. The dashed curve is the transmission for calcium over a range of SW values and the solid curve is the transmission for argon. The first pair of vertical lines indicates the IS associated SW speed range and the second set of vertical lines indicates the transmission for the CH associated SW speed range. Clearly, the total transmission for calcium is much higher than the total transmission for argon in the two SW speed ranges. This dif-

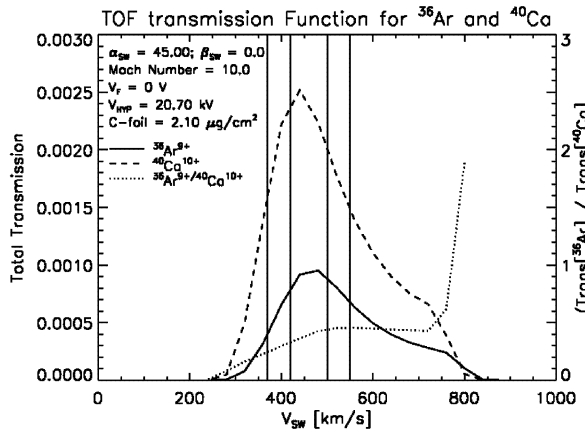


**FIGURE 1.** The isochronous TOF mass spectrometer total transmission is plotted for argon and calcium investigated in this study. The approximate MTOF sensor settings and the general SW values are located in the upper left-hand corner. The total transmission of argon is indicated with the solid line and calcium is represented with the dashed line. The first pair of vertical lines indicates the IS associated SW bin while the second set of vertical lines indicates the CH associated SW bin. The dotted curve gives the transmission ratio of  $^{36}\text{Ar}$  to  $^{40}\text{Ca}$ .

ference is the result of the larger yield of positive ions after the carbon foil from calcium than argon. The dotted curve indicates the transmission ratio of  $^{36}\text{Ar}$  to  $^{40}\text{Ca}$ . This curve graphically shows how calcium is more efficiently detected than argon. This difference in transmissions is accounted for by taking the mean transmission ratio of calcium to argon in both speed ranges, which is 3.45 for the IS associated SW bin and 2.22 for the CH associated SW range.

Table 1 lists the instrument settings required for the selection of data for the two different SW speed ranges. Again, these settings are selected to maximize the SNR for the argon peaks in the Weygand et al. [11] study, to examine the two compositionally different SW regimes, and to maximize the particle's transmission through the instrument.

Data from 1996 to the first half of 1999 are examined and the selected mass spectra are summed together to make one total mass spectrum for each SW speed range. For the IS associated SW the summed spectra amounts to 3.6 days worth of data. For the CH associated SW the summed spectra is for 5.6 days worth of data. The total number of days appears to be low because the entrance system settings are not always ideal and a minimum of 12 hours worth of IS associated solar wind (or a minimum of 6 hours of CH associated SW) are required to guarantee a pure sample. Figure 2 shows the compiled mass spectrum for the IS associated speed SW and Figure 3 displays the mass spectrum for the CH associated SW, respectively. On the figure's top half within the spectra seven mass

**TABLE 1.** MTOF sensor instrumental settings for different SW bins.

Portion of MTOF Sensor	Interstream Associated SW 370 to 420 km/s	CH Associated SW 500 to 550 km/s
Acceleration	0.0	0.0
Voltage ( $V_f$ )		
Hyperbola Voltage	20.4 kV	20.4 kV
Entrance	4.9 to 7.9 kV	8.0 to 12.4 kV
System Voltage		
Min SW	12 hr	6 hr
Speed Duration		
N/S SW Angle	$\pm 8^\circ$	$\pm 8^\circ$
Mach Number	$\geq 10.0$	$\geq 0.0$

peaks are visible, which are  $^{34}\text{S}$ ,  $^{35}\text{Cl}$ ,  $^{36}\text{Ar}$ ,  $^{37}\text{Cl}$ ,  $^{38}\text{Ar}$ ,  $^{39}\text{K}$ , and  $^{40}\text{Ca}$ . Along the x-axis is the TOF channel number, along the y-axis is the total number of counts per channel, the thin black line indicates the raw data, and the thick curve is a 16 parameter Maximum Likelihood fit (MLF) to the spectrum. The MLF is explained in detail in the study of Bochsler et al. [17]. The difference in this study is we have only seven mass peaks and we fit a quadratic background. The bottom part of each figure is a plot of the relative difference of the raw spectrum from the fit spectrum ( $(\text{Raw} - \text{Fit})/\text{Raw}$ ). It should be clear from the lower plot how good the fit is and relative difference variations above and below zero indicates that we are not consistently fitting above or below the raw data. The residuals are basically random, thus no systematic error in the fit and the fit function selection has been made. As a MLF consistency check, the Ar/Ca fit ratio was compared with the Ar/Ca raw count ratio and the ratios are consistent within the uncertainty.

## RESULTS AND DISCUSSION

Displayed in Table 2 are the argon to calcium ratios derived from the IS and CH associated SW spectra along with the results of other studies. An examination of the previously published Ar/Ca ratios shows the scatter of the Ar/Ca values as well as the large uncertainty of these determinations. The ratios for this study represent the ratio of the area under the argon peaks and the calcium peaks. While only the area under the  $^{36}\text{Ar}$  and  $^{40}\text{Ca}$  peaks is determined, the various isotopes of calcium and argon are accounted for by using the isotopic abundance ratios. In addition to the  $^{36}\text{Ar}$  peak there is an  $^{38}\text{Ar}$  peak, which is difficult to see in Figure 2.  $^{40}\text{Ar}$  also exists within the SW, but its overall contribution is negligible. An argon isotopic ratio ( $^{36}\text{Ar}/^{38}\text{Ar}$ ) for the IS associated SW of 5.6 is used to determine the area under the  $^{38}\text{Ar}$  peak and an argon isotopic ratio of 5.5 is used for the CH associ-

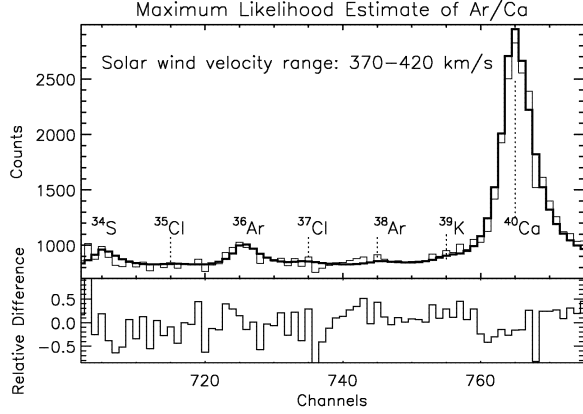


**FIGURE 2.** The plot's top half is the sum of the five minute mass spectra between 1996 and 1999 for the IS associated SW range of 370 km/s to 420 km/s. The thin black line represents the raw data and the thick black line is the MLF of the argon peaks. Along the Y-axis is the counts, along the X-axis are the TOF channel, and each isotope is labelled above each peak. The dotted line indicates the peaks position. The plot's bottom half is the relative difference between the fit and raw counts.

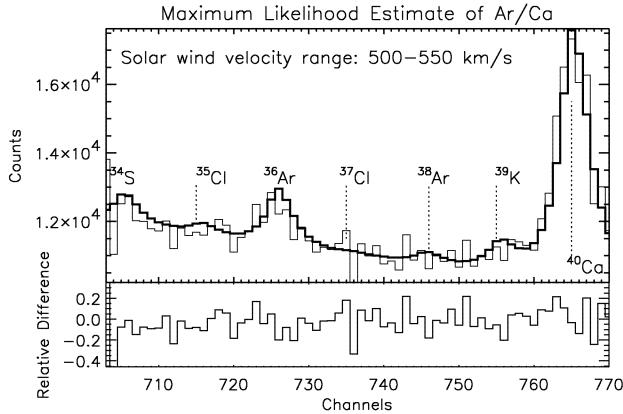


**FIGURE 3.** Same as Figure 2, but for SW speeds from 500 km/s to 550 km/s.

ated SW bin [11]. Like argon, calcium has more than one peak,  $^{42}\text{Ca}$  and  $^{44}\text{Ca}$ , which are not shown in either Figure 2 or 3. Calcium isotopic ratios are used to calculate the area under those calcium peaks [18]. An additional correction is made to account for the difference in calcium and argon transmission through the TOF portion of the instrument as discussed in the procedure section (see also Figure 1).

At this time, it is appropriate to explain the method of determination for the Ar/Ca ratio absolute uncertainty. The IS associated SW background for both elements is estimated to have a relative uncertainty of 3.6% ( $\sqrt{n}/n$ , where  $n$  is the background counts). For the CH associated SW the background is 0.9% for argon and 1.0%

**TABLE 2.** Ar/Ca elemental abundance ratios for this work and previous studies.

Measured Regime	Ar/Ca Ratio	Reference
<b>In situ SW</b>		
IS SW	$0.38 \pm 0.05$	This Work
CH SW	$0.59 \pm 0.07$	This Work
<b>Optical (Flare)</b>		
EUV Flare Data	$0.55 \pm 0.21$	Widing & Spicer [19]
EUV Flare Data	$1.10 \pm 0.25$	Widing & Hiei [20]
Impulsive Flare Data	$1.5 \pm 0.8$	Feldman & Widing [21]
Flare Data	$0.79^{+0.54}_{-0.45}$	Veck & Parkinson [22]
<b>Optical (Other)</b>		
Photosphere, Coronal SEP data Spectroscopy	$1.10 \pm 0.14$	Grevesse & Sauval [23]
CI Chondrites (Ca) Photosphere Spectroscopy (Ar)	$1.65 \pm 0.15$ $1.58 \pm 0.41$	Anders & Grevesse [3]
Coronal Spectra	$0.85 \pm 0.20$	Young et al. [24]
<b>Energetic particles</b>		
SEP Derived Corona	$0.30^{+0.74}_{-0.63}$	Breneman & Stone [2]
SEP Derived Corona	$0.31 \pm 0.02$	Reames [4]
Mass Unbiased Baseline SEP	$0.71 \pm 0.70$	Meyer, [25]

for the calcium. The instrumental relative uncertainty for the entrance system of MTOF, according to carbon foil area variation for different elemental charges, is approximately 5.0% for the IS associated SW and about 3.8% for the CH associated SW. The instrumental relative uncertainty for the TOF portion of MTOF is 7% in the elemental discrimination due to the release of start electrons, 5% for the uncertainty in the elemental discrimination due to charge state conversion in the carbon foil, and 7% in the elemental discrimination due to the stop detection efficiency. The area under the IS associated SW peaks has a relative uncertainty of approximately 3.2% for the  $^{36}\text{Ar}$  peak and 2.6% for the  $^{40}\text{Ca}$  peak. For the area under the coronal hole associated SW spectrum peak we find about 1.2% and 0.6% relative uncertainty for the  $^{36}\text{Ar}$  and  $^{40}\text{Ca}$  peak, respectively. A final uncertainty of 12% and 10% is included for the  $^{36}\text{Ar}/^{38}\text{Ar}$  isotopic ratio in the IS and

CH associated speed SW regimes, respectively. The sum of the squares of the uncertainties results in a total relative uncertainty of about 13.3% for the IS associated SW value and about 11.8% for the CH associated SW value. Unfortunately, these uncertainties are not expected to improve much with the addition of more MTOF data. Only a moderate improvement could be made by further restricting the sensor settings and with the accumulation of a much larger number of spectra.

The IS associated SW Ar/Ca ratio of this work  $0.38 \pm 0.05$  is consistent with the results of the Breneman and Stone [2], Meyer [25], and Reames [4] studies. These results, which are derived from SEP measurements, are believed to reflect the mean composition for the IS associated SW and the coronal composition. The IS associated SW value of this work, as well as the other SEP results, are not consistent with the work of Young et al. [24].

The results of this work for the CH associated SW Ar/Ca ratio  $0.59 \pm 0.07$  is consistent with the Widing and Spicer [19] work's results as well as the Veck and Parkinson [22] studies. These previously published studies are believed to reflect the mean composition for the CH associated SW. We should also point out that the CH associated SW value of this study falls within the uncertainty of the Meyer [25] and the Young et al. [24] works, which are believed to reflect IS associated SW results. The purpose of this comment is to emphasize the highly variable values and large uncertainties associated with previous studies. The IS associated SW value of this work is not consistent with the work of Grevesse and Sauval [23]. The reason our value may be different from the Grevesse and Sauval [23] study is that they use sunspot data, solar corona data, and SW particle data to derive an argon photospheric abundance and that work does not have a direct photospheric value.

It is interesting to note that the Ar/Ca published values averaged together for the composition representative of the photosphere (1.16) is greater than the Ar/Ca average ratio (0.54) representative of the published interstream associated SW by a factor of about 2.1. Similarly, the IS associated SW ratio of this study is less than the CH associated SW Ar/Ca ratio by a factor of also 1.6. This difference is most likely due to FIP type fractionation which occurs in the solar atmosphere. The details of this process are still unclear at this time. This ratio of CH associated SW to the IS associated SW is similar in nature to that factor found in the Aellig et al. [10] and Wurz et al. [9] studies, where the O/Fe elemental ratio in the IS associated SW is about a factor of 1.82 less than in the CH associated SW. For this work, we have inverted the Aellig et al. [10] study Fe/O elemental abundance ratio to simplify the comparison of a high FIP element to a low FIP species. For the Bochsler et al. [17] study, a FIP factor of 2.1 is reported, where the difference

between the Al/Mg elemental abundance ratio in the IS and CH associated SW is examined. While it is known that the  $[X/O]_{ISSW}/[X/O]_{CHSW}$  varies for each element, the purpose of the above discussion is to indicate that we find FIP fractionation of 1.6, which is a typical FIP fractionation pattern between the IS and CH associated SW.

The difference between the Ar/Ca IS and CH associated SW has one of three implications. The first option is the argon abundance is constant in all SW regimes and the calcium is depleted in the CH associated SW, which is suggested in the research of Meyer [26], Veck and Parkinson [22], and Raymond et al. [27, 28]. This theory is supported by the results of Wurz [12], which demonstrates a decrease in the calcium abundance on the order of 60% in the SW. This abundance decrease is sufficient to explain the factor of 1.6 difference in the MLF counts. The second option is that the argon abundance is depleted in the IS associated SW and the calcium abundance remains unchanged. This has been suggested in the work of Marsch et al. [29] and Peter [30]. The third option is both abundances change in the SW, with the abundance of the low-FIP element stronger than the high-FIP element. This has been observed for O, Si, and Fe abundances [12].

## CONCLUSIONS

The Ar/Ca elemental ratios for the IS and CH associated SW of this study are consistent with many previously published values determined from gradual SEP events, optical spectroscopy, the Apollo foil experiment results, and from meteorites. The IS associated SW Ar/Ca elemental ratio of  $0.38 \pm 0.05$  is a factor of 1.6 larger than the CH associated SW Ar/Ca elemental ratio of  $0.59 \pm 0.07$ . This difference can be easily understood in terms of the FIP fractionation process. The difference between the two SW bin's Ar/Ca ratios suggest that either the argon is enhanced in the CH associated SW or the calcium is depleted in the CH associated SW with respect to the IS associated SW.

The uncertainty for these values is generally smaller than the Ar/Ca ratio found in the gradual SEP event studies and significantly smaller than the uncertainty related to spectroscopic Ar/Ca ratios. Slight improvements to the uncertainty can be made in the future by collecting more spectra as CELIAS/MTOF gathers more data and by tightening the data selection. Unfortunately, the measurement uncertainty for the ratios within this work are large and are not expected to improve by more than a few percent, because of the significant instrumental uncertainty. The most significant improvement of these observations over the previous ones is these measurements

represent direct samples from two different SW regimes, and they tie a volatile element to a refractory element, as opposed to previous investigations that determined the ratio indirectly from the solar wind or the solar atmosphere. Furthermore, we place limits on the Ar/Ca elemental abundance ratio variability directly in the contemporary SW under different SW conditions.

## ACKNOWLEDGMENTS

This work is supported by the Swiss National Science Foundation. CELIAS is a joint effort of five hardware institutions under the direction of the Max-Planck Institut für Extraterrestrische Physik (pre-launch) and the University of Bern (post-launch).

## REFERENCES

1. Cerutti, H., *Die Bestimmung des Argons im Sonnenwind aus Messungen an den Apollo - SWC - Folien*, Ph.D. thesis, University of Bern, Bern, Switzerland (1974).
2. Breneman, H., and Stone, E., *Astrophys. J.*, **299**, L57–L61 (1985).
3. Anders, E., and Gevesse, N., *Geochim. Cosmochim. Acta*, **53**, 197–214 (1989).
4. Reames, D., *Space Sci. Rev.*, **85**, 327–340 (1998).
5. Gloeckler, G., Balsiger, H., Bürgi, A., Bochsler, P., Fisk, L. A., Galvin, A. B., Geiss, J., Gliem, F., Hamilton, D. C., Holzer, T. E., Hovestadt, D., Ipavich, F. M., Kirsch, E., Lundgren, R. A., Ogilvie, K. W., Sheldon, R. B., and Wilken, B., *Space Sci. Rev.*, **71**, 79–124 (1995).
6. Hovestadt, D., Hilchenbach, H., Bürgi, A., Laeverenz, B. K. P., Scholer, M., Grünwaldt, H., W. I. Axford, S. L., Marsch, E., Wilken, B., Winterhoff, P., Ipavich, F. M., Bedini, P., Coplan, M. A., Galvin, A. B., Gloeckler, G., Bochsler, P., Balsiger, H., Fischer, J., Geiss, J., Kallenbach, R., Wurz, P., Reiche, K. U., Gliem, F., Judge, D. L., Hsieh, K. C., Möbius, E., Lee, M. A., Managadze, G. G., Verigin, M. I., and Neugebauer, M., *Solar Physics*, **162**, 441–481 (1995).
7. Gloeckler, G., Cain, J., Ipavich, F. M., Tums, E. O., Bedini, P., Fisk, L. A., Zurbuchen, T., Bochsler, P., Fischer, J., Wimmer-Schweingruber, R. F., Geiss, J., and Kallenbach, R., *Space Sci. Rev.*, **86**, 497–539 (1998).
8. Kern, O., Wimmer-Schweingruber, R. F., Bochsler, P., Gloeckler, G., and Hamilton, D. C., *ESA*, **SP-415**, 345–348 (1997).
9. Wurz, P., Aellig, M. R., Ipavich, F. M., Hefti, S., Bochsler, P., Galvin, A. B., Grünwaldt, H., Hilchenbach, M., Gliem, F., and Hovestadt, D., *Phys. Chem. Earth*, **24**, 421–426 (1999).
10. Aellig, M. R., Hefti, S., Grünwaldt, H., Bochsler, P., Wurz, P., Ipavich, F. M., and Hovestadt, D., *J. Geophys. Res.*, **104**, 24769–24780 (1999).
11. Weygand, J. M., Ipavich, F. M., Wurz, P., Paquette, J. A., and Bochsler, P., *Geochim. Cosmochim.* (2001), (in press).
12. Wurz, P., *Heavy Ions in the solar wind: Results from SOHO/CELIAS/MTOF*, Habilitation thesis, University of Bern, Bern, Switzerland (1999).
13. Neukomm, R. O., *Composition of coronal mass ejections derived with SWICS/Ulysses*, Ph.D. thesis, University of Bern, Bern, Switzerland (1998).
14. Wurz, P., Ipavich, F. M., Galvin, A. B., Bochsler, P., Aellig, M. R., Kallenbach, R., Hovestadt, D., Grünwaldt, H., Hilchenbach, M., Axford, W. I., Balsiger, H., Bürgi, A., Coplan, M. A., J. Geiss, F. G., Gloeckler, G., Hefti, S., Hsieh, K. C., Klecker, B., Lee, M. A., Livi, S., Managadze, G. G., Marsch, E., Möbius, E., Neugebauer, M., Reiche, K. U., Scholer, M., Verigin, M. I., and Wilken, B., *Geophys. Res. Lett.*, **25**, 2557–2560 (1998).
15. Wurz, P., Wimmer-Schweingruber, R., Issautier, K., Bochsler, P., Galvin, A., and Ipavich, F., (these proceedings).
16. Bürgi, A., Gonin, M., Oetliker, M., Bochsler, P., Geiss, J., Lamy, T., Brenac, A., Andrä, H. J., Roncin, P., Laurent, H., and Coplan, M. A., *J. Appl. Phys.*, **73**, 4130–4139 (1993).
17. Bochsler, P., Ipavich, F. M., Paquette, J. A., Weygand, J. M., and Wurz, P., *J. Geophys. Res.*, **105**, 12659–12666 (2000).
18. Kallenbach, R., Ipavich, F. M., Bochsler, P., Hefti, S., Wurz, P., Aellig, M. R., Galvin, A. B., Geiss, J., Gliem, F., Gloeckler, G., Grünwaldt, H., Hilchenbach, H., Hovestadt, D., and Klecker, B., *Astrophys. J.*, **498**, L75–L78 (1998).
19. Widing, K., and Spicer, D., *Astrophys. J.*, **242**, 1243–1256 (1980).
20. Widing, K., and Hiei, E., *Astrophys. J.*, **281**, 426–434 (1981).
21. Feldman, U., and Widing, K., *Astrophys. J.*, **363**, 292–298 (1990).
22. Veck, N. J., and Parkison, J. H., *MNRAS*, **197**, 41–55 (1981).
23. Gevesse, N., and Sauval, A. J., *Space Sci. Rev.*, **85**, 161–174 (1998).
24. Young, P. R., Mason, H. E., Feenan, F. P., and Widing, K. G., *Astron. Astrophys.*, **323**, 243–249 (1997).
25. Meyer, J. P., *Ap. J. Suppl. Ser.*, **57**, 151–171 (1985a).
26. Meyer, J. P., *Ap. J. Suppl. Ser.*, **57**, 173–204 (1985b).
27. Raymond, J. C., Kohl, J. L., Noci, G., Antonucci, E., Tondello, G., Huber, M. C. E., Gardner, L. D., Nicolosi, P., Fineschi, S., Romoli, M., Spadaro, D., Siegmund, O. H. W., Benna, C., Ciaravella, A., Cranmer, S., Giordano, S., Karovska, M., Martin, R., Michels, J., Modigliani, A., Naletto, G., Panasyuk, A., Pernechele, C., Poletto, G., Smith, P. L., Suleiman, R. M., Strachan, L., and van Ballegooijen, A. A., *Solar Physics*, **175**, 645–665 (1997).
28. Raymond, J. C., Suleiman, R., Kohl, J. L., and Noci, G., *Space Sci. Rev.*, **85**, 283–289 (1998).
29. Marsch, E., von Steiger, R., and Bochsler, P., *Astron. Astrophys.*, **301**, 261–276 (1995).
30. Peter, H., *Astron. Astrophys.*, **312**, L37–L40 (1996).